Simulation of the photocatalytic removal of stearic acid discrete deposits on the surface of a non-porous titania thin film

Nouari Chaoui, Yann Battie, Fouad Araiedh

Version of Record: https://www.sciencedirect.com/science/article/pii/S1385894719332954
Manuscript_0724c8727a7343983714a9ebbd062ea6

Simulation of the photocatalytic removal of stearic acid discrete deposits on the surface of a non-porous titania thin film

Nouari CHAOUI[a,*], Yann BATTIE[a] and Fouad ARAIEDH[b]

[a] Laboratoire de Chimie et Physique-Approche Multi-échelle des Milieux Complexes (LCP-A2MC), Université de Lorraine, France.

[b] Unité de Recherche Catalyse et Matériaux pour l'Environnement et les Procédés (URCMEP), Université de Gabès, Tunisie.

Abstract

We apply a kinetic model to simulate the photocatalytic removal of stearic acid (SA) discrete deposits. At the microscopic scale, the SA deposit is modelled as a set of hundreds of squared islands deposited on the TiO_2 surface and separated from each other. The input data include the projected areas and heights of the islands both characterized by a Gaussian distribution law with a mean value and various standard deviations. The effects of these parameters are examined, analyzed and put in relation with experimental results from the literature. The dependence of the removal kinetics of the SA deposits on its initial microstructure is clearly demonstrated. Additionally, we show that the removal kinetics of the SA deposit as measured by infrared spectroscopy can be satisfactory predicted from the distributions of the initial projected areas of the islands and their heights as measured by optical microscopy and atomic force microscopy.

Keywords : Titania, Photocatalysis, Self-cleaning, Stearic acid, Kinetic model

***Corresponding author :**

Laboratoire de Chimie et Physique - Approche Multi-échelle des milieux complexes (LCP-A2MC) Université de Lorraine - Institut Universitaire de Moselle est - Département « Science et Génie des Matériaux » 5, rue Camille Weiss 57600 Forbach

Tel. : + 33 3 72 74 98 38 Fax : + 33 3 72 74 98 30 email : nouari.chaoui@univ-lorraine.fr

1. Introduction

Past and current developments in photocatalysis on semiconductor surface have led to applications in numerous areas and especially in the removal of air pollutants [1,2,3] and waste-water treatment [4,5]. This might explain why most of the reports dedicated to mechanisms and kinetics in photocatalysis often concerns liquid and gas phases. In these two latter cases, the Langmuir-Hinshelwood (L-H) model [6,7] is the most commonly applied model. However, the application of photocatalysis in the area of self-cleaning surfaces [8,9] raised issues concerning the photocatalytic removal mechanisms and kinetics of organic substances *in the solid phase* such as soot [10,11,12,13,14] or fatty acids [15,16,17,18,19]. While the L-H model is *entirely* rationalized *at the molecular level* by the surface adsorption, diffusion and reaction of two molecules, the situation is drastically different when it comes to degradation of *a solid deposit* on a photocatalyst surface [20].

At the molecular scale, the photocatalyzed degradation of a solid organic deposit on titanium dioxide surface in presence of dioxygen can be summarized by the following reaction [15,16]:

$$\text{Organic} + x\text{O}_2 \rightarrow y\text{CO}_2 + z\text{H}_2\text{O} + \text{mineral acids} \quad (2)$$

This reaction can only occur in the presence of oxygen and UV-light with photon energy superior to the band gap of anatase, i.e. >3.2 eV. The photocatalytic degradation may be the result of a direct reaction with a photogenerated carrier (electron or hole) and/or that of an indirect reaction with radical species resulting from the reaction of adsorbed species (O_2 or H_2O) and photogenerated carriers on the photocatalyst surface. In many cases, these processes occurring *at the molecular level* are not sufficient to rationalize the removal kinetics of solid organic deposits and the overall description of the degradation process requires a multiscale approach.

In the particular case of fatty acids, depending on the deposition method and conditions, the obtained deposit can take the form of micrometric islands on the TiO_2 surface. In a previous work [21], using both optical and atomic force microscopies, we observed such a discrete structure on a stearic acid deposit prepared by dip-coating. We showed that photocatalytic degradation of an individual island followed a zero-order kinetics while that of the overall deposit, as measured by infrared spectrometry, showed an apparent first-order behavior. To explain these discrepancies, we proposed a kinetic model which takes into account the projected areas and heights of each island as measured by optical microscopy and atomic force microscopy. Using this model, we concluded that the apparent first-order behavior was a consequence of the microstructure. In recent reports [22], David Ollis classified and analyzed all the possible deposit/film configurations of the literature including that previously described and concluded that almost all the photocatalyzed degradation rates of the fatty acid deposit can be empirically described by a power law with the general form :

$$Rate = k_{cat}[C]^n$$

n is the apparent reaction order and k_{cat} a fundamental constant of the photocatalyst which is independent on [C]. The author concluded that the apparent reaction order n was closely related to the initial size distribution of the islands. He showed that three possible values for n, i.e. 0, 1/2 or 1 whether the initial size distribution of islands is monodisperse, presents a narrow distribution or a broad distribution, respectively.

The main objective of this work is to assess the impact of the initial microstructure of the SA discrete deposit on its removal kinetics. To this end, we simulate the photocatalytic degradation of a set of hundreds microscopic squared SA islands presenting various microstructures. The results of the simulations are compared

to the results of the literature and for each case the apparent reaction order is determined and discussed.

2. The kinetic model

2.1 Optical microscope examination of a SA deposit prior to UV light exposure

The kinetic model is initially based on the observation of a SA deposit on a sol-gel TiO_2 thin film using optical microscopy. Fig. 1 shows a representative microscopy image of such a deposit.

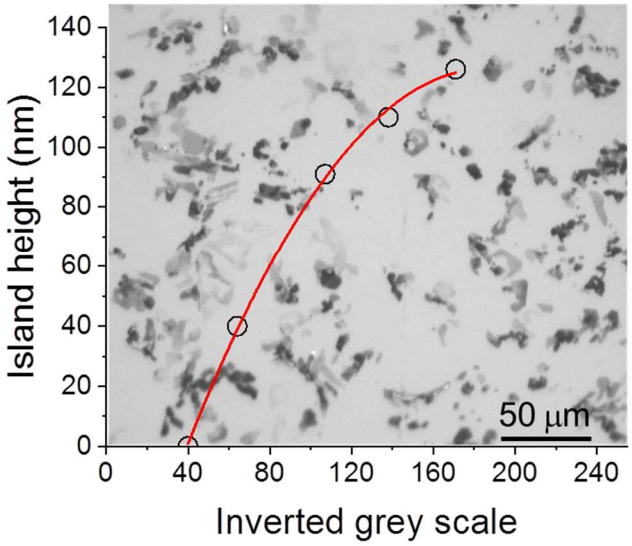

Figure 1: Optical microscopy image of a SA deposit on the surface of a non-porous titania film. The superimposed graph represents the islands height, as measured by atomic force microscopy, as a function of the inverted grey scale of the microscopic image.

At the microscopic scale, it was observed that the SA deposit consists of irregularly shaped islands with Feret diameter ranging from few µm up to the order of ten µm and various grey levels. We also noticed a correlation between the grey scale of the microscope image and the islands height as measured by atomic force microscopy [21]. The island height as a function of the inverted grey scale is shown in Fig. 1. In reflected light microscopy, the image contrast is mainly due to partial absorption and/or scattering of the incident light rays which are both related to the thickness of the

specimen (SA islands) and the optical properties of the specimen. However, the observed contrast cannot only be understood in terms of interaction of the incident light rays with the SA islands. The image processing including adjustment of the brightness and contrast makes the physical relationship between the grey scale and the height of the islands not trivial. Therefore, the evolution shown in Fig. 1 has been empirically fitted with a polynomial law. As the inverted grey scale value increases from 40 (image background) to about 100 the islands height evolves almost linearly from 0 to 90 nm. Above 150 which correspond to black pixels the height becomes less sensitive to the grey scale. From the microscopy image, the set of islands can be roughly sorted in three classes of grey levels: black, dark grey and light grey islands corresponding to level above 150, between 100 and 150, and below 100, respectively. According to Fig. 1, the black islands present an average height of 120 nm, the dark grey ones 90 nm and the light grey ones 60 nm. The AFM measurements have shown that the height of the islands do not exceed 150 nm.

2.2 Dependence of the disappearance rate of an island on its height

Figure 2 (a) and (b) presents the projected area of three islands with similar initial values and different heights as a function of exposure duration to UV light.

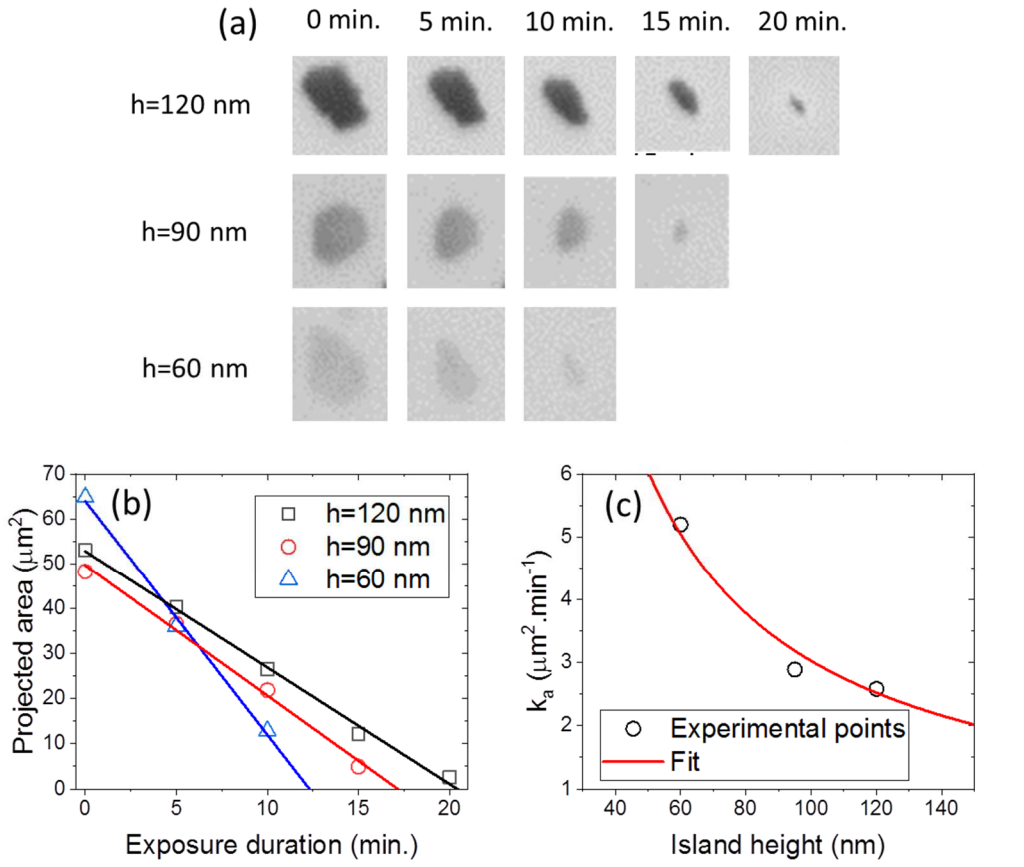

Figure 2: (a) Microscopic images of three islands with similar initial values but different heights at different stages of the photocatalytic degradation process. (b) Projected area of these three islands as a function of exposure duration to UV light. (c) Rate of area loss of an island as a function of its height. The experimental points have been fitted by a hyperbolic function.

It is observed that the projected area of the islands (Fig. 2(a)) gradually decreases from the border towards the centre with a constant rate (Fig. 2(b)). In agreement with the work of Zaleska et al [23], It was also found that the island height remained constant during the photocatalytic degradation process owing to their grey level which remains unchanged (Fig. 2(a)). Furthermore, it clearly appears from both microscopic images (Fig. 2(a)) and time evolutions of the projected areas (Fig. 2(b)) that the rate of area loss

varies inversely with islands height. Taking into account these experimental facts, the rate of area loss can be written:

$$-\frac{da}{dt} = k_a(h) \quad (1)$$

where $k_a(h)$ is a rate constant which depends on island height.

Fig. 2 (c) presents the rate of area loss of an island as a function of island height (points) obtained from Fig. 2(b). The rate of area loss is assumed to be inversely proportional to the island height. This implies that the rate of area loss tends towards infinity as the island height approaches zero and vice et versa. This assumption is reasonable in the light of Fig. 2 (a) and 2 (b) and is also consistent with the findings of Allain et al [24] who reported a similar behaviour when plotting SA kinetic constant as a function of initial SA amount (in $mol.cm^{-2}$) on mesoporous TiO_2 samples.

The fact that the height remains constant during the photocatalytic degradation process implies that the rate of volume loss of the island is also constant. Consequently, the removal rate of an island should also obey to a zero-order kinetic law with respect to mass. In view of the above, the experimental points (Fig. 2(c)) have been fitted by a hyperbolic function (red line):

$$k_a = \frac{288}{h} \quad (2)$$

According to eq. (1), the fitting parameter is expressed in $\mu m^2.min^{-1}.nm^{-1}$. Eq. (2) represents the dependence of the rate of area removal as a function of island height.

2.3 Simulation of the mass loss of a set of islands

The basic principle of the model is sketched in Fig. 3. According to eq. (1), the rate of area loss of an island i with a height h_i among a set of n islands, as observed under the microscope can be written:

$$-\frac{da_i}{dt} = k_a(h_i) \quad (3)$$

Integration of eq. (3) conducts to the projected area of an island i as a function of an exposure duration t to UV light which writes:

$$a_i(t) = -k_a t + a_{i0} \quad (4)$$

where a_{i0} is the the initial projected area.

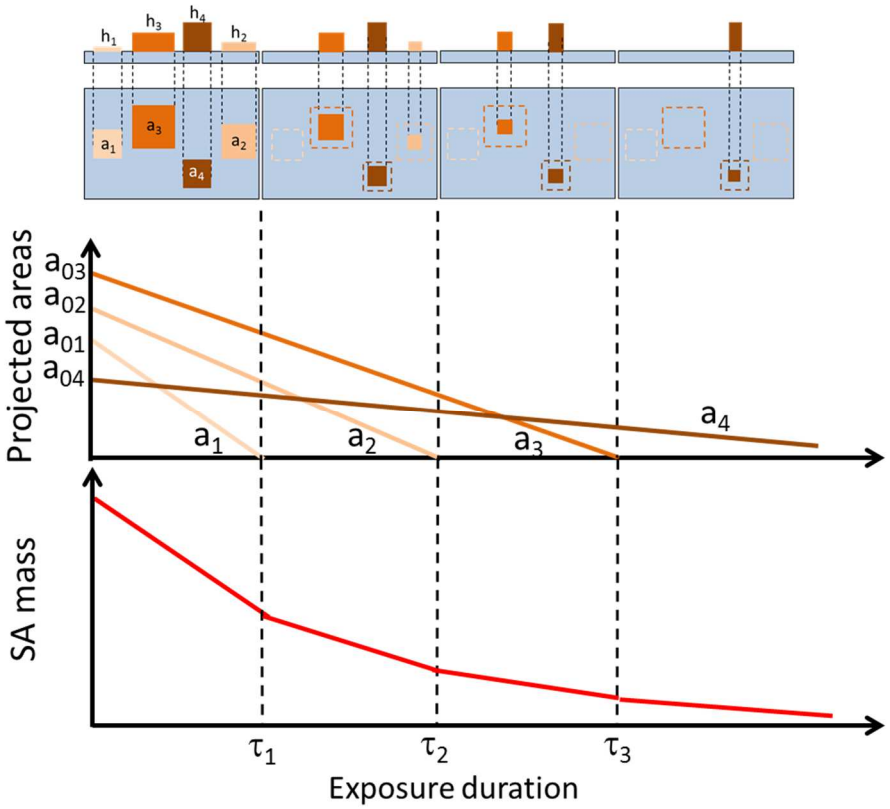

Figure 3: Schematic of the basic principle of the model.

A given island i contributes to the mass loss of the deposit until it completely disappears after an exposure duration τ_i (Fig. 3), i.e. its lifetime. To take into account the finite lifetime of island i, eq (4) is multiplied by the Heaviside function $H(\tau_i - t)$:

$$a_i(t) = (-k_a t + a_{i0}) \times H(\tau_i - t) \quad (5)$$

The term $H(\tau_i - t)$ cancels the equation as soon as $t = \tau_i$ i.e., as soon as $\tau_i = a_{i0}/k_a$. The mass $m_i(t)$ of an island as a function of exposure duration then writes:

$$m_i(t) = \rho h_i(-k_a t + a_{i0}) \times H(\tau_i - t) \quad (6)$$

Where ρ is the SA density. The remaining mass m(t) of a set of n islands after an exposure duration t to UV light can be expressed as the sum of masses of the n islands:

$$m(t) = \sum_{i=1}^{n} m_i(t) = \sum_{i=1}^{n} [\rho h_i(-k_a t + a_{i0}) \times H(\tau_i - t)] \quad (7)$$

Eq. (7) offers a direct link between the projected areas of the islands as measured by microscopy and the mass of the deposit as measured by FTIR spectrometry, the integrated absorbance of the infrared region being proportional to SA mass.

3. **Simulations**

The scheme in Fig. 4 summarizes the model parameters and the input data. The deposit is modelled as a set of 500 hundred square islands spread on the TiO_2 surface and separated from each other (Fig. 4(a)).

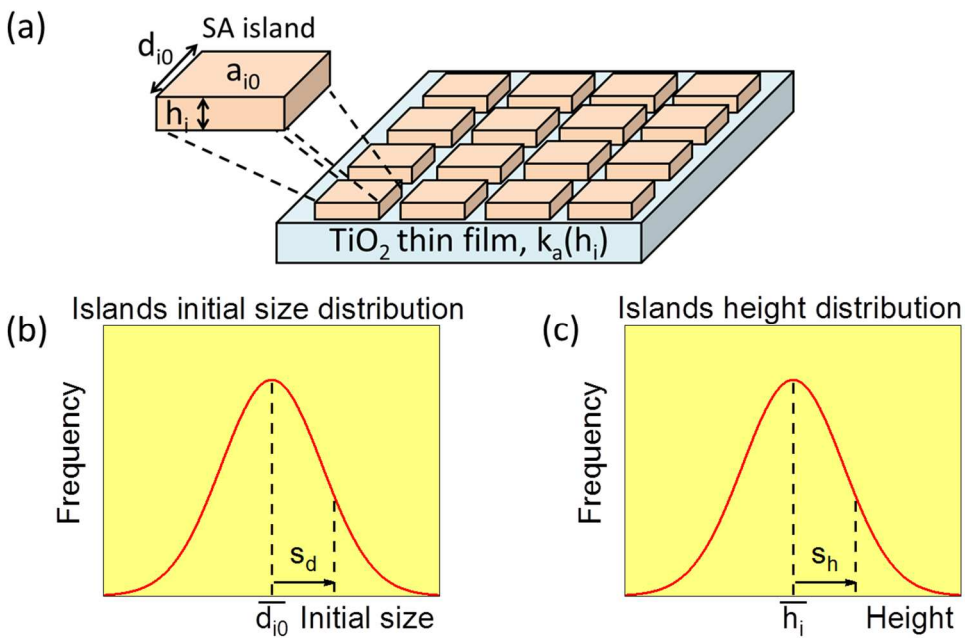

Figure 4: Definitions of the model parameters and input data.

The input data include the initial sizes $d_{i0,}$ (side length at t=0) of the square islands from which are calculated their projected areas $a_{i0} = d_{i0}^2$ and the islands heights h_i (Fig. 4(a)). The initial sizes and heights of the islands are characterized by a Gaussian distribution law (Figs. 4(b) and (c)) with a mean value ($\overline{a_{i0}}$ and $\overline{h_{i,}}$, respectively) a standard deviation (s_d and s_h, respectively). The input data also include the rate of area loss $k_a(h_i)$ as a function of islands height which can be viewed as a property of the TiO_2 film calculated according to eq. (2). The time evolution of the mass of the islands set in then calculated using equation (7). Since the IR absorbance is proportional to mass, the time evolution of the mass can then be easily converted in a time evolution of IR absorbance.

3.1 Case n°1 : effect of the size distribution of the islands

The first studied configuration concerns a set of SA islands of equal heights h_i and Gaussian initial size distributions characterized by a mean value of $\overline{d_{i0}} = 5$ µm and various standard deviations s_d. Figure 5 presents the calculated mass evolution of the

islands set as a function of exposure duration to UV light for several values of heights ranging from 5 to 200 nm. In Fig. 5(a), a set of monodispersed (s_d=0 µm) islands is first considered.

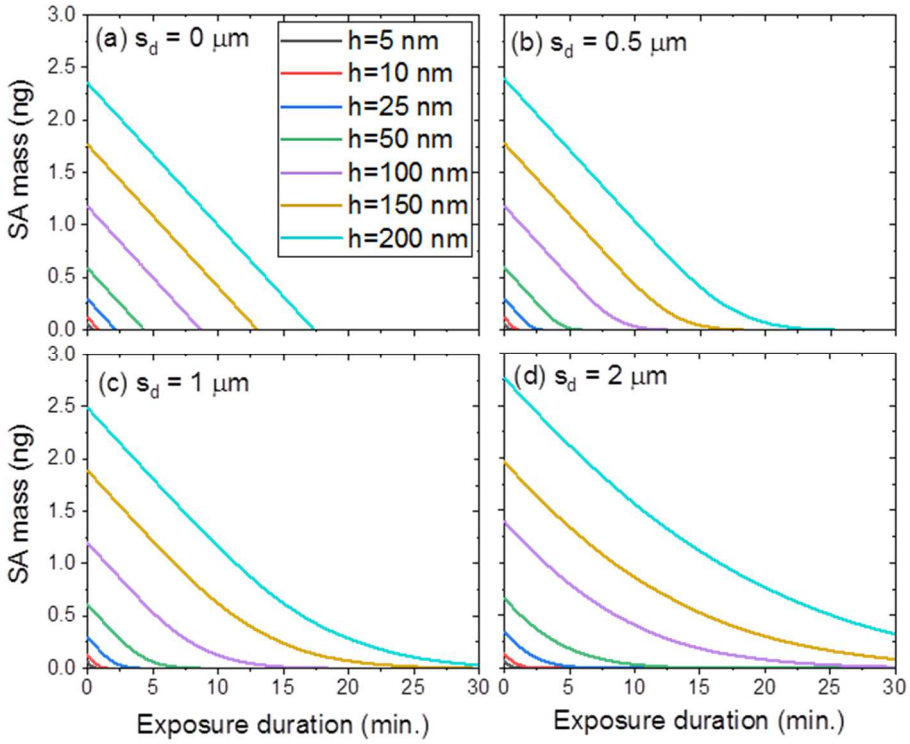

Figure 5: Calculated mass of a set of SA islands as a function of exposure duration to UV light for a monodispersed islands set with initial size of d_{i0}=5 µm (a) and for islands set presenting a Gaussian size distribution with initial mean size $\overline{d_{i0}}$=5 µm and standard deviations s_d =0.5 µm (b), s_d =1 µm (c) and s_d =2 µm (d). In each case, the calculation was performed for several height values ranging from 5 to 200 nm.

When the islands size distribution is monodispersed (Fig. 5(a)), the evolution of the mass of the deposit follows a linear law with the same slope, i.e. removal rate of the deposit, whatever the height of the island population. This can be explained by the fact that each island disappears with the same rate with respect to SA mass and equally contributes to the overall mass loss throughout the exposure duration. In contrast, as

the initial size of the islands is no longer monodisperse (Fig. 5(b)), the evolution is still initially linear but deviates from linearity at a late stage of the exposure to UV light so that the time evolution of the SA mass can be divided in two regimes: a zero-order regime and a non-linear regime. As the distribution broadens (Figs. 5(c)-(d)), it is found that the inflection point between the two regimes shifts towards short exposure durations (Fig. 5(d)) so that the non-linear regime tends to dominate the SA mass evolution. The broadening of the islands size distribution results in a growing number of small islands which increasingly contribute to the overall SA mass. Since their lifetimes are shorter [21], the effect of their total disappearance on the overall SA mass evolution is observed earlier.

This configuration is similar to that reported by Zaleska et al [23] on the removal of lauric acid (LA) deposited on an anatase single crystal. Using atomic force microscopy, these authors reported that prior to UV exposure the deposit consisted of a non-continuous film with domains structure consisting of networks of interconnected LA blocks of the order of ten micrometres in size and an almost monodispersed height distribution (in the range 80-90 nm). They measured the evolution of the *surface coverage* of the deposit as a function of exposure duration to UV light and claimed a linear decrease. However, a close inspection of the late stage of the evolution clearly shows a deviation from linearity just before the total disappearance of the deposit similar to that presented in Fig. 5(b).

3.2 Case n°2 : effect of the height distribution of the islands

The second case concerns a set of SA islands presenting the same initial size d_{io} and a Gaussian height distribution characterized by a mean value $\overline{h_i}$=100 nm and by various standard deviation s_h. Figure 6 presents the calculated mass of such islands set as a

function of exposure duration for several initial sizes ranging from 2 to 10 µm. In Fig. 6(a), a set of monodisperse (s_h=0 nm) islands in with a height of h_i =100 nm is first considered. Then, the calculated mass of a set of islands with a Gaussian height distribution with a mean height of $\bar{h}_i = 100$ nm and standard deviations of s_h =10 nm, s_h =20 nm and s_h =40 nm are plotted against exposure duration to UV light in Figs. 6(b), (c) and (d), respectively.

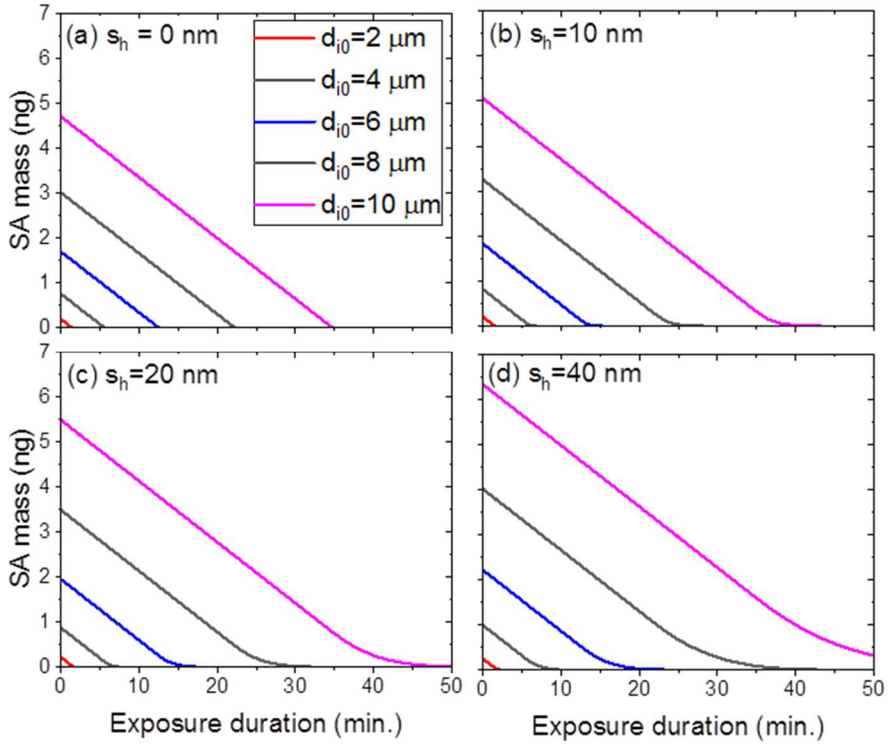

Figure 6: Calculated mass of a set of 500 stearic acid square islands as a function of exposure duration to UV light for a monodispersed population of islands with a height of h=100 nm (a), for a population of islands presenting a Gaussian height distribution with a mean height of $\bar{h} = 100$ nm and a standard deviation of s_h =10 nm (b), s_h =20 nm (c) and s_h =40 nm (d) for several initial size values d_{i0} ranging from 2 to 10 µm.

The first configuration (Fig. 6(a)) is similar to that described in Fig. 5(a) and the same arguments can be invoked to justify the observed zero-order kinetic. When the heights

distribution slightly broadens (Fig. 6(b)), here again, the evolution of the SA mass gently deviates from the linear behaviour just before the total disappearance of the deposit. As in the previous case, the overall SA mass evolution can be divided in two regimes: a zero- order regime and a non-linear regime and the broader the height distribution, the earlier occurs the transition between the two regimes (Figs. 6(c) and (d)). The behaviour of the overall SA mass can be explained by the gradual disappearance of the lower islands that have shorter lifetimes. It may also be noted that compared to the effect of size distribution, the impact of the islands height distribution on the SA mass evolution is less significant. This can be explained by the almost 2D morphology of the islands. Their height is typically one order magnitude than their sizes. This explains why the height variations have a lower impact on the island volume and mass than that of the size.

In order to further illustrate the effect of islands height distribution on the evolution of the overall SA mass another height distribution was considered. This one concerns a set of 500 islands having all the same initial size d_{i0}=5 μm ($a_{i0} = 25\ \mu m^2$) but presenting polymodal height distributions with 2 (5, 10 nm) to 8 modes (5 nm, 10 nm, 15 nm,…, 40 nm) each one being monodisperse. Figure 7 shows the calculated mass of the islands set as a function of exposure duration to UV light.

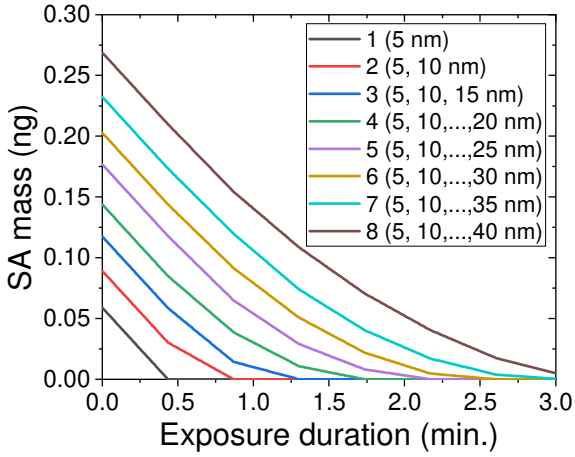

Figure 7 : Calculated mass of a set of 500 stearic acid square islands as a function of exposure duration to UV light for a set of islands with a monodispersed initial size (d_{i0}=5 µm) and a polymodal height distribution each mode being monodisperse. The figures in the legend refer to the number of modes and the values in brackets indicate the height associated with each mode. The number of islands per mode is the same.

It is observed that for a bimodal (5 nm, 10 nm) height distribution, the evolution is initially linear but shows a slope break after half of the require time for the total removal of the deposit. While the slope at the initial stage corresponds to the simultaneous contribution of both modes to the overall mass loss, the second one corresponds to the gradual removal of the remaining parts of the islands of the second mode. Therefore, the slope break marks the total disappearance of the first mode (5 nm). This explanation can be generalized to the other polymodal distributions. For a given number of modes N, the number of slope breaks is then (N-1). Each slope break marks the lifetime of the islands of a given mode. As the number of modes increases, the slope breaks become less discernible so that the SA mass evolution presents a concavity which is consistent with first-order behaviour.

3.3. Case n°3: combined effect of size and height distributions

The last case concerns a set of SA islands presenting both height and size Gaussian distribution having a mean height $\overline{h_i}$=100 nm, a mean size $\overline{d_{oi}} = 5$ µm and standard deviations s_h and s_d. Figure 8 presents the calculated mass evolution of such islands set as a function of exposure duration for various values of s_h and s_d.

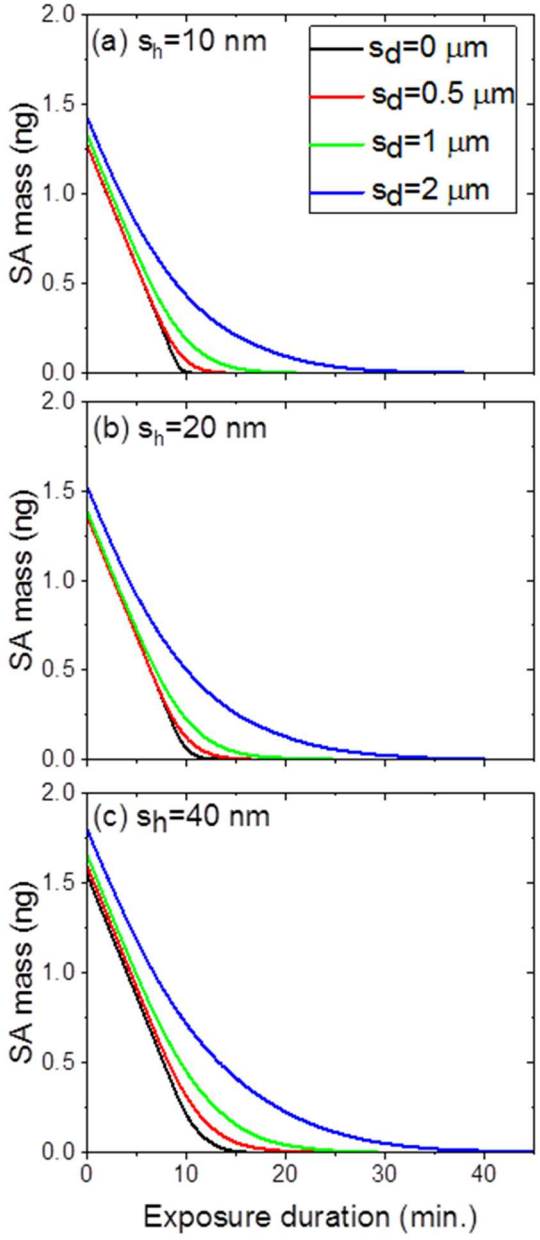

Figure 8: Calculated mass of a set of 500 stearic acid square islands as a function of exposure duration to UV light. The islands population presents a Gaussian distribution

in size and height. The height distribution is characterized by a mean height of $\bar{h} =$ 100 nm and standard deviations of s_h =10 nm (a), s_h =20 nm (b) and s_h =40 nm (c). The size distribution is characterized by a mean size of $\overline{d_{ol}} = 5$ µm and several standard deviations ranging from 0 to 2 µm.

For a narrow heights distribution (Fig. 8(a)), the time evolution of the total SA mass is almost linear (black line) but gradually moves to an apparent first-order kinetics (blue line) when s_d increases. As the height distribution widens (Fig. 8(b) and (c)), the evolution of the SA mass follows apparently first-order kinetics even for narrow size distribution and for a given height distribution the concavity of the curves is all the more pronounced as the size distribution broadens. This configuration is comparable to the experimental results reported by Sawunyama et al [25]. These authors studied the degradation of a 25 nm-thick SA layer deposited on titania using the Langmuir-Blodgett method. Using atomic force microscopy, they showed that the removal proceeded via the collapse of the initially continuous SA layer which led to the formation of an "island-like" structure with broad size and height distribution. The resulting SA islands were on the order of the micrometre in size and achieve 30 nm in height. From the time evolution of the IR absorbance in the 2800-3000 cm^{-1} region, they showed that the overall reaction proceeded via first-order kinetics the behaviour of which is in a good agreement with the simulation results presented in Fig. 8(c).

4. Application of the model to our experimental results

In the following, the kinetic model is applied to our experimental results [21] with a view to link the time evolution of the projected surface area of each island as measured by optical microscopy to that of the global SA mass as measured by FTIR spectrometry. As previously mentioned, the set of SA islands was divided in three groups, i.e. black,

dark grey and light grey islands corresponding to average heights of 120, 90 and 60 nm according to Fig. 1. The height distribution is then assumed to be trimodal and the size distribution of the islands within each of the three categories was determined by image processing. Fig. 9 presents binarized images corresponding to each mode and the projected surface area distributions of the islands in number frequency. Only the islands with surface area above 1 μm^2 were considered in order to avoid the inclusion of the artefacts from the image background.

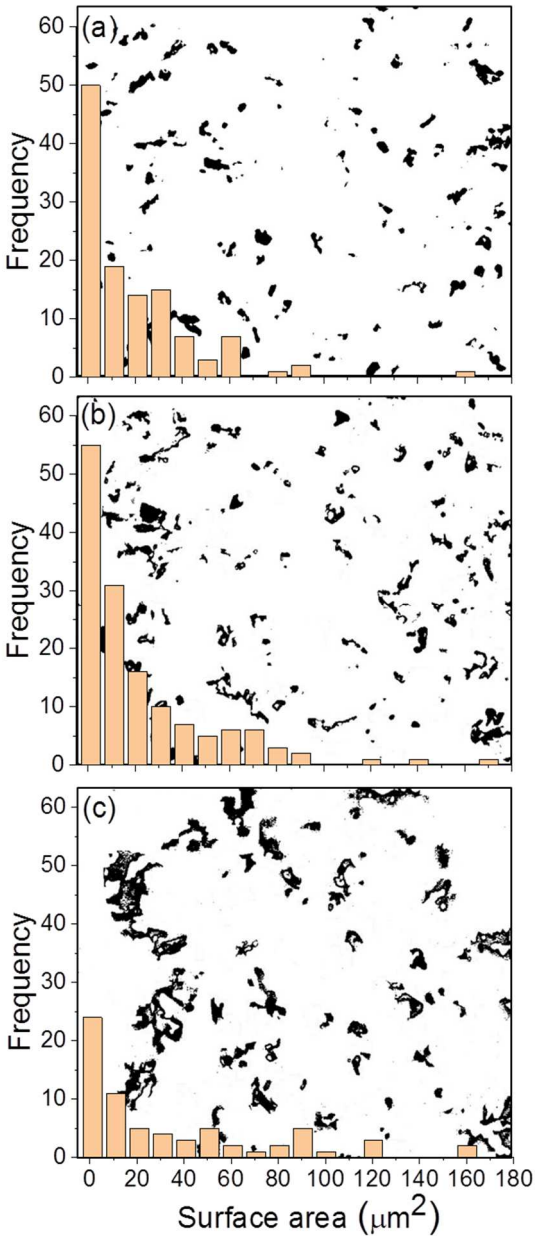

Figure 9: Processed image of the SA deposit of the islands (Fig. 1). The islands heights are sorted in three modes 120 nm (a), 90 nm (b) and 60 nm (c) after application of thresholds using the graph of Fig. 1 and conversion to binary image. The histograms associated to each image represent the projected areas distributions of the islands in number frequency.

As a first step, the SA mass evolution of each mode has been separately calculated and plotted as a function of UV exposure time. The obtained results are presented in Fig. 10(a). Each of these three evolutions is consistent with the previously described case N°2.

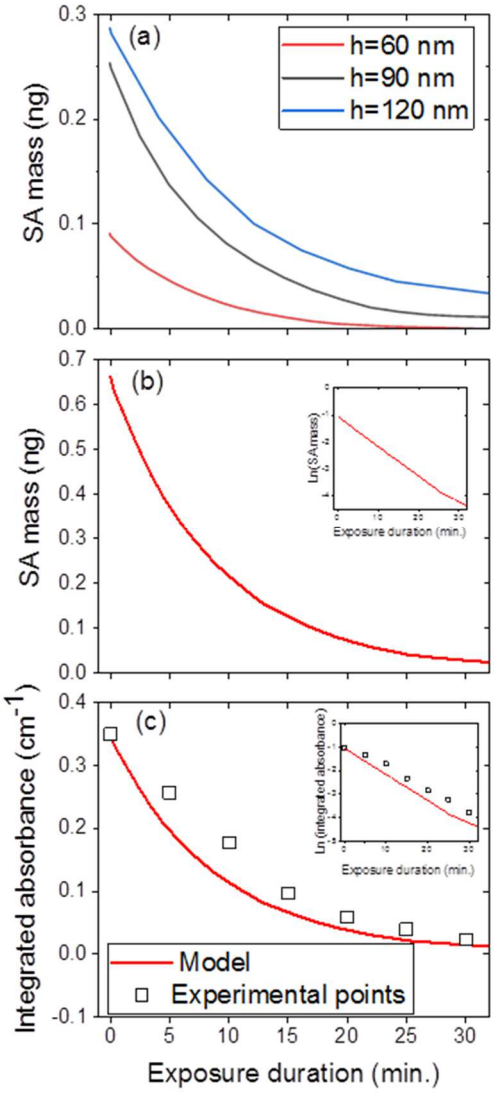

Figure 10: Calculated mass evolution as a function of exposure duration to UV light for the data shown in Fig. 9 of (a) each height mode, (b) overall SA deposit. (c) Calculated and experimental integrated IR absorbance of the SA deposit. The insets in Figs. 10 (b) and (c) represent the logarithm of the SA mass and the logarithm of the integrated IR absorbance, respectively.

The time evolution of the overall SA mass was obtained by summing the contribution of each mode (Fig. 10(a)). As shown in Fig. 10(b), the resulting evolution follows a pseudo first-order kinetic law with respect to SA mass as confirmed by the linear evolution of logarithm of the time evolution of the SA mass (Fig. 10(b), inset). In order to compare the time evolution of the calculated SA mass (Fig. 10(b)) to that measured by IR spectrometry [21], the plots of Fig. 10(b) have been converted into integrated IR absorbance (Fig. 10(c)). This conversion was performed by multiplying the SA mass by a normalization factor f=0.527 $cm^{-1}.ng^{-1}$ which is the ratio between the integrated IR absorbance A_0=0.349 cm^{-1} (Fig. 10(c)) and the calculated SA mass m_0=0.662 ng (Fig. 10 (b)) at t=0. The calculated and experimental values are found to be in satisfactory agreement. As shown in inset of Fig. 10 (c), the apparent kinetic constants are found to be 0.100 and 0.093 $cm^{-1}.min^{-1}$ for the calculated and experimental values, respectively. However, it appears that the calculated values somewhat underestimate the measured values and especially at the early stage of the UV light exposure. Several reasons can be invoked to explain the observed discrepancy. On one hand, the latter may be due to the uncertainties related to the measurements of the surface areas of the islands due to the resolution limit of the microscope and the image processing. While the thresholding step of the grey level image is rather easy for the black and dark grey islands that concerning the light grey islands (h=60 nm) is more complicated because of the low contrast between the islands and the image background. This explanation is consistent with the

fact that the difference between the calculated and experimental values is larger at the early stage of the UV exposure. At this stage, the light grey islands contribute significantly to the mass loss of the SA deposit. Similarly, given the fact that the grey level of the microscope images is sharply correlated to the height as show in Fig. 1, it is likely that a significant part of the SA mass come from islands with heights clearly below 60 nm that cannot be distinguished from the image background by lack of contrast. Furthermore, as previously shown [21], SA islands, as observed by optical microscopy, appear slightly smaller than the same islands observed by AFM and this particularly applies for thinner islands. Besides, the islands with surface area above 1 μm^2 were considered in order to avoid the artefacts from the image background. These ones may also significantly contribute to the overall mass loss during the early stage of the degradation process. Lastly, we assumed in the model that the islands with different sizes and heights are isolated from one another. However, the microscope images show that many islands with different sizes and heights are interconnected but the calculated evolution of the mass of the deposit neglects these interconnections. This also may explain the overestimation of the calculated degradation rate at the beginning of the process.

As a conclusion, simulations of the photocatalytic degradation of stearic acid microscopic islands were performed. Several initial size/height distributions are examined and the obtained results are put in relation with previously reported experimental results. One of the most relevant results is the fact that the removal kinetics of a SA deposit as measured by infrared spectroscopy can be predicted with a satisfactory accuracy from the initial islands size/height distribution as measured by optical and/or atomic force microscopies. The dependence of the removal of the SA

deposits on its initial morphology at the microscopic scale is clearly demonstrated. The results of the simulation show that the photodegradation of the deposit follows a zero-order kinetic with respect to SA mass when the size *and* height distribution of the island set is monodisperse. In contrast, it tends towards an apparent first-order law when the size and/or height distribution of the islands set becomes broader. An intermediate situation for which the time evolution of the SA mass which is initially linear but deviates from linearity at latter stage, is also revealed for narrow size and/or height distributions. The position of the inflection point between the two regimes was found to be correlated to the distribution width. As the latter increases, the inflection point shifts towards short exposure durations. These observations confirm the analyses of the literature results recently reported by D. Ollis [22].

Acknowledgement

This work has been supported by the Erasmus Mundus Program E-GOV-TN (European Union - Project n° 2013-2434). F.A. is grateful to the consortium for funding of his PhD thesis.

References

[1] J. Peral, D. F. Ollis, J. Catal. **136** (1992) 554-565

[2] N. Keller, M.N. Ducamp, D. Robert, V. Keller, Chem Rev. **113** (2013), 5029-5070.

[3] J. Mo, Y. Zhang, Q. Xu, J. J Lamson, R. Zhao, Atm. Environ. **43** (2009) 2229-2246

[4] O. Alfano, D. Bahnemann, A. Cassano, R. Dillert, R. Goslich, Catal. Today **58** (2000) 199-230

[5] S. Malato, P. Fernández-Ibáñez, M. Maldonado, J. Blanco, W. Gernjak, Catal. Today **147** (2009) 1-59

[6] A.L. Pruden, D.F. Ollis J. Catal. **67** (1981) 35; J. Catal. **82** (1983) 404

[7] J.M. Herrmann, Applied. Catal B: Environn. **99** (2010) 461-468

[8] A. Heller, Acc. Chem. Res. **28** (1995) 503-508

[9] A. Fujishima, K. Hashimoto, T. Watanabe TiO_2 Photocatalysis : Fundamentals and Applications, BKC, Inc., Tokyo, 1999

[10] M. C. Lee, W. Choi, J. Phys. Chem. B **106** (2002) 11818-11822

[11] S. K. Lee, S. McIntyre, A. Mills, J. Photochem. Photobiol. A: Chemistry **162** (2004) 203-206.

[12] A. Mills, J. Wang, M. Crow, Chemosphere **64** (2006) 1032-1035

[13] P. Chin, G. W. Roberts, D.F. Ollis, Ind. Eng. Chem. Res. **46** (2007) 7598-7604; P. Chin, C.S. Grant, D.F. Ollis Appl. Catal. B **87** (2009) 220-229

[14] Y. Kameya, K. Torii, S. Hirai, M. Kaviany, Chemical Engineering Journal **327** (2017) 831-837

[15] Y. Paz, Z. Luo, L. Rabenberg, A. Heller, J. Mat. Res. **10** (1995) 2842 – 2848 ; Y. Paz, A. Heller, J. Mat. Res. **12** (1997) 2759 – 2766.

[16] A. Mills, A. Lepre, N. Elliott, S. Bhopal, I.P. Parkin, S. A. O'Neill, J. Photochem. Photobiol. A: Chemistry **160** (2003) 213-224; A. Mills, J. Wang, J. Photochem. Photobiol. A: Chemistry **182** (2006) 181-186; A. Mills, M. Mcfarlane, Catalysis Today 129 (2007) 22-28

[17] L. Peruchon, E. Puzenat, A. Girard-Egrot, L. Blum, J.M. Hermann, C. Guillard, J. Photochem. Photobiol. A: Chemistry **197** (2008) 170-176.

[18] V. Roméas, P. Pichat, C. Guilard, T. Chopin, C. Lehaut, New J. Chem. **23** (1999) 365-373.

[19] J. T. Remillard, J.R. McBride, K. ; E. Nietering, A.R. Drews, X. Zhang, J. Phys. Chem. **104** (2000) 4440-4447.

[20] D. Ollis, Appl. Catal. B : Environ. **99** (2010) 478-484.

[21] M. N. Ghazzal , N. Barthen and N. Chaoui, Appl. Catal. B: Environ. **103** (2011) 85-90.

[22] D. Ollis, Appl. Catal. B : Environ. **209** (2017) 174-182 ; Appl. Catal. B : Environ. **242** (2019) 431-440.

[23] A. Zaleska, J. Nalaskowski, J. Hupka, J.D. Miller Appl. Catal. B : Environ. **88** (2009) 407-412

[24] E. Allain, S. Besson, C. Durand, M. Moreau, T. Gacoin, J.-P. Boileau, Adv. Funct. Mater. **17** (2007) 549-554.

[25] P. Sawunyama, L. Jiang, A. Fujishima, K. Hashimoto, J. Phys. Chem. **101** (1997) 11000-11003.

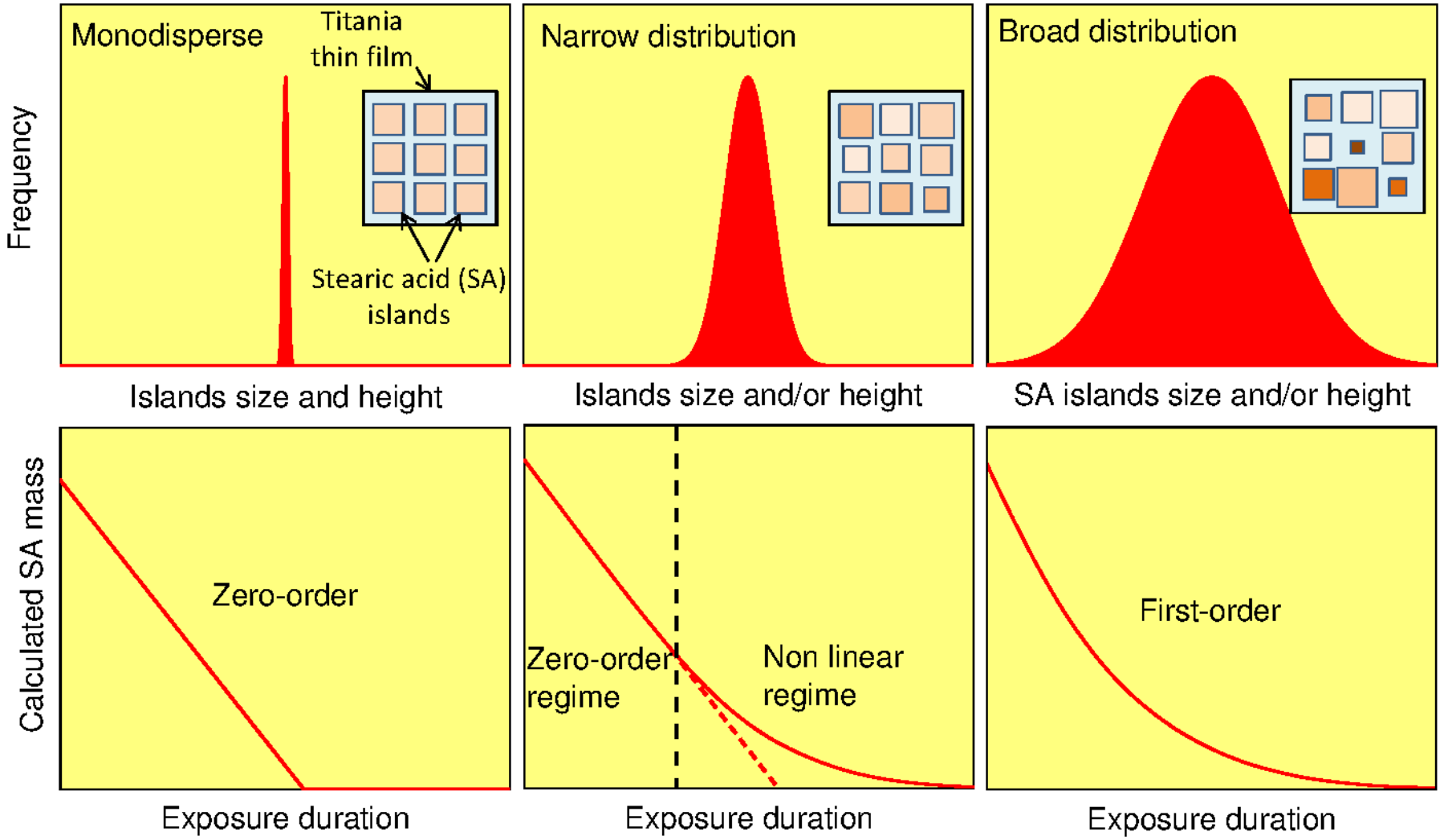
Frequency
Monodisperse
Titania
thin film
Stearic acid (SA)
islands
Narrow distribution
Broad distribution
Islands size and height
Islands size and/or height
SA islands size and/or height
Calculated SA mass
Zero-order
Zero-order
regime
Non linear
regime
First-order
Exposure duration
Exposure duration
Exposure duration